Heat Transfer from the Stagnation area of a heated Cylinder at Re_D = 140 000 affected by free-stream turbulence

J.G. Wissink[a], W. Rodi[b]

[a]*School of Engineering and Design, Brunel University, Kingston Lane, Uxbridge, UB8 3PH, UK, e-mail: jan.wissink@brunel.ac.uk*
[b]*Institute for Hydromechanics, KIT, Kaiserstr. 12, D-76128 Karlsruhe, Germany*

Abstract

The effect of free-stream grid-turbulence on the flow around and heat transfer from the stagnation region of a circular cylinder was studied using Direct numerical simulations (DNS). Simulations with and without free-stream fluctuations were carried out at a Reynolds number of $Re_D = 140\,000$ (based on the inflow velocity and the cylinder diameter D), which is in the higher subcritical range. A splitter plate was introduced behind the cylinder to counteract the formation of a vortex street. To resolve the flow up to 746.5 million grid points were employed. Compared to the fully laminar simulation, the addition of $Tu = 30\%$ grid turbulence at the inflow plane was found to lead to an increase in heat transfer at the stagnation line of the cylinder of 66%. A very good agreement was obtained with the correlations of Dullenkopf & Mayle (J. Turbomachinery **116**, 1994 & J. Turbomachinery **117**, 1995).

Keywords: heat transfer, Free-stream turbulence, stagnation region flow

1. Introduction

The temperature at which a turbine can be operated is limited by the material used for the manufacturing of the blades and the effectiveness of the blade-cooling strategy. A peak in the heat load on turbine blades is reached in the stagnation region, where - due to the strongly accelerating external flow - the boundary layer is laminar. External fluctuations, originating from the upstream row of blades, that impinge on the stagnation-region-boundary-layer will lead to an increase in heat transfer. The latter is referred to as ”laminar heat transfer”.

The stagnation region of a circular cylinder is very similar to the stagnation region of a turbine blade. This is why there have been many experimental studies of laminar heat transfer from/to the stagnation region of cylinders induced by incoming turbulence. Our aim is to add to these studies by performing a DNS of this heat transfer problem at a relatively high Reynolds number. Because of the aforementioned similarity in shape, the findings of this DNS are directly transferable to the fluctuation-induced increase in heat transfer to the stagnation region of turbine blades.

Several experiments have been performed to study the influence of free-stream turbulence on laminar heat transfer and on boundary layer transition. In their experimental studies of laminar heat transfer along a flat plate affected by free-stream fluctuations, Kestin et al [1] and Junkhan and Serovy [2] discovered that in order for these fluctuations to be able to increase heat transfer, the affected laminar boundary layer flow needs to be accelerating. These findings were confirmed by the experiments of Schulz [3], who measured the heat transfer distributions around a typical fore-loaded airfoil for several free-stream turbulence levels.

More recently, van Fossen et al [4] performed a series of experiments of flow and heat transfer in the stagnation region of a body with an elliptical leading edge. Based on these experiments they showed that laminar heat transfer tends to increase with both the turbulence intensity, Tu, and the Reynolds number but decreases with the integral length-scale of the grid turbulence. Ames et al [5] reported experimental results on the effects of various levels of inlet turbulence on the surface of a vane at exit Reynolds numbers between $Re = 500\,000$ and $2\,000\,000$. Both turbulence level and scale were shown to affect heat transfer augmentation and the heat transfer increase was found to scale with $Re_D^{5/12}$.

Xiong and Lele [6] performed a theoretical analysis of the distortion of two-dimensional stagnation point flow by three-dimensional disturbances as well as their influence on the heat transfer enhancement. The most effective disturbances were found to have a length scale that was close to five times the boundary-layer thickness, which is somewhat smaller than the ratio of $9 - 10$ that was found by Dullenkopf and Mayle [7] and Yardi and Sukhatme [8]. Dullenkopf and Mayle [9, 7] have proposed correlations for the heat transfer enhancements based on earlier measurements on cylinders and airfoils, first without [9] and then with [7] including the effect of the length scale of the turbulence. These correlations will be used for comparison with the simulations in the present study.

The first DNS involving laminar heat transfer from a heated turbine blade was performed by Wissink and Rodi [10]. The DNS showed a moderate increase

in heat transfer in the laminar portion of the boundary layer that could be attributed to the presence of free-stream fluctuations. A study of stagnation point flow and fluctuation-induced heat transfer using LES was performed by Xiong and Lele [11]. Intense quasi-streamwise vortices were found to develop near the leading edge leading to turbulent heat flux to peak much closer to the wall than the Reynolds stresses. Wissink and Rodi [12] performed the first DNS in which the influence of an incoming turbulent wake on stagnation heat transfer from an heated cylinder was studied. A Reynolds number of $Re_D = 13\,200$, based on the free-stream velocity and the diameter of the cylinder, was employed. The results showed a strong correlation between the augmentation of free-stream heat transfer and the instantaneous turbulence level of the oncoming flow. We would like to refer to this paper for an extensive literature review on laminar heat transfer induced by free stream fluctuations. Compared to Wissink and Rodi [12], the present paper studies the effect of oncoming grid turbulence, rather than turbulence in a wake, on stagnation heat transfer and employs a significantly higher Reynolds number.

Dullenkopf and Mayle [9], van Fossen et al [4] and Ames et al [5] all predicted the fluctuation-induced stagnation heat transfer to increase with the Reynolds number Re_D. As a result, in our DNS study we chose to use a fairly high Reynolds number of $Re_D = 140\,000$ - based on the free-stream velocity U_0 and the diameter of the cylinder D - in order to find a significant increase in stagnation heat transfer. With the DNS presented in this paper, which fully resolves the fluctuation-induced heat transfer process in the stagnation region, we aim to produce good quality data 1) to elucidate/confirm the physical mechanisms that play a role in laminar heat transfer and 2) to serve as reference data with which to improve heat transfer models. By employing such improved models in industrial codes, a more accurate prediction of the heat load in the stagnation region of turbine blades can be achieved and more efficient blades can be designed.

2. Computational Details

2.1. Numerical Aspects

The three-dimensional, incompressible Navier-Stokes equations were discretised using a collocated, curvilinear finite-volume code that combined a second-order central discretisation in space with a three-stage Runge-Kutta method for the time-integration. In the 3D DNS reported here, $2406 \times 606 \times 512$ grid points were used in the circumferential, radial, and spanwise direction, respectively. The code was parallelised using the standard Message Passing Interface (MPI) protocol. For a more detailed description of the code see Breuer and Rodi [13].

The (spanwise cross-section of the) computational geometry is shown in Figure 1. The free-stream temperature is $T_\infty = 0.7T_0$, where T_0 is the cylinder wall temperature. At the inflow plane a flow field $(u, v, w)^t = (1, 0, 0)^t U_0 + (u', v', w')^t$ was prescribed, in which the free-stream fluctuations $(u', v', w')^t$ originated from a separate large-eddy simulation of isotropic turbulence in a box. As shown in Table 1, two simulations were performed. In the 3D turbulent DNS (Simulation II) the turbulence intensity $Tu = \sqrt{\frac{1}{3}\frac{\overline{u'u'}+\overline{v'v'}+\overline{w'w'}}{U_0^2}} \times 100\%$ at the inflow plane was set to a high value of $Tu_{in} = 30\%$ in order to retain a reasonably increased turbulence level of 3.5% close to the cylinder, while in the quasi-2D laminar baseline DNS (Simulation I) $Tu_{in} = 0\%$. The spanwise size of the Simulation II was $l_z/D = 0.6$ and the integral length-scale of the free-stream fluctuations was approximately $\frac{1}{10}l_z$. At the upper and lower boundaries free-slip boundary conditions were used while at the surface of the cylinder a no-slip condition was employed. At the outflow plane a convective outflow condition was used and in the spanwise direction of the 3D simulation periodic boundary conditions were employed. The splitter plate (with free-slip boundary conditions) mounted behind the cylinder was used to counteract the formation of a von Karman vortex street behind the cylinder that might cause a quasi-periodic motion of the stagnation line at the front of the cylinder. To save grid points, the size of the computational domain was chosen as small as possible without compromising the accuracy of the calculations: Based on experience gained in previous simulations, the distance between the inflow plane and the axis of the cylinder was chosen to be $5D$, which is long enough to justify the assumption of a uniform mean flow field. Also, the absence of a von Karman vortex street behind the cylinder allowed us to select a relatively short outflow region of only $5D$.

In Figure 2 a detail of the O-mesh in the (x, y) plane employed in both simulations is shown. Because of the dense grid, only every twelfth grid-line is displayed. It can be seen that the grid near the cylinder is only stretched in the radial direction. This was done to avoid the occurrence of numerical inaccuracies due to unfavourable cell aspect ratios. Towards the boundary of the computational domain the circular shape of the circumferential direction of the O-mesh is smoothly changed into a rectangular shape. As a result, in almost the entire computational domain the shape of the grid volumes is near-optimal, while only the volumes in the outer corners - which are far enough away to not have any effect on the flow around the cylinder - have a less favourable shape. The radial distance between the wall-nearest computational point and the wall in wall-units is less than $r^+ = 0.9$ and the point to point distances in the circumferential and spanwise directions are

less than $\phi^+ = 15.6$ and $z^+ = 14.0$, respectively. The time step employed in the simulations is $\delta t = 5 \times 10^{-5} D/U_0$.

An overview of the two DNS performed is given in Table 1, detailing the number of grid points in the circumferential, the radial and the spanwise directions, respectively. In Simulation II a total of 746.5 million grid points were employed.

3. Results

3.1. General flow characteristics

3.1.1. Time-averaged statistics of the flow field

Figure 3 shows streamlines of the time-averaged flow field from Simulation II. The stagnation line is identified by the label "St". In the upper half of the figure, the primary re-circulation area is identified by "V", while "W" identifies a small secondary re-circulation zone. "S", finally, corresponds to the saddle point that marks the maximum downstream extent of the recirculation zones. Note that the two major re-circulation areas are separated by the splitter plate, which prevents any interaction between them. In the absence of incoming turbulence (Simulation I) the boundary layer was found to separate about 74^o from the stagnation point. In Simulation II, the boundary layer was energized by the incoming turbulence, which resulted in a delay of the separation to about 83.5^o from the stagnation point.

Boundary layer profiles at various locations in, and immediately downstream of, the stagnation region from the laminar Simulation I and the turbulent Simulation II are compared in Figure 4. The good agreement obtained at all locations illustrates the fact that, despite the presence of free-stream turbulence in the incoming flow, the boundary layer remains laminar also in Simulation II.

The profiles of the total and fluctuation-induced shear stress, displayed in Figure 5 illustrate that the contribution of the fluctuation-induced shear to the total shear is quite small. Also this indicates that,though the boundary layer is slightly energised by external disturbances, it remains laminar.

Figure 6 displays the decay of the intensity of isotropic turbulence introduced at the inflow plane along $y/D = 0$. Immediately downstream of the inflow plane a sharp drop (caused by interpolation errors) in the Tu-level from $Tu_{in} = 30\%$ to $Tu = 25\%$ can be observed. After a transient behaviour between $x/D = -5$ and $x/D = -4.7$, Tu is observed to approximately undergo an exponential decay until it reaches a minimum value of $Tu = 3.5\%$ at $x/D = -0.75$.

3.1.2. Instantaneous flow patterns

Figure 7 shows contours of a snapshot of the circumferential velocity fluctuations from Simulation II in a plane at a distance of $0.00065D$ to the surface of the cylinder, which is located in the lower part of the boundary layer. In the region where the flow is attached, the interaction of external fluctuations with the boundary layer flow can be seen to result in a pattern of longitudinal disturbances. In the region behind the cylinder, the pattern significantly changes and becomes far more fine-grained, indicating the presence of turbulent motion close to the cylinder's surface.

Figure 8 shows instantaneous vorticity contours in the plane at mid-span. The free-stream turbulence can be seen to consist of small vortical structures whose intensity decays from the inlet plane towards the cylinder. The shear in the separating boundary layers at the top and bottom of the cylinder can be clearly identified by its intense vorticity that quickly declines in the downstream direction due to the high level of turbulence that is present inside the large re-circulation regions. Near the location of stagnation the fluctuating velocity vector-field, shown in Figure 9, illustrates the presence of relatively large spanwise eddies with a diameter comparable with the integral length scale, $\Lambda \approx 0.057D$, of the free-stream turbulence. Very close to the cylinder the spanwise eddies tend to disappear. This can be partially explained by the strongly accelerating flow immediately upstream of the front of the cylinder, which quickly convects the spanwise eddies over the top or bottom half of the cylinder.

The quotient of the integral length scale, $\Lambda \approx 0.057D$, and the boundary layer thickness δ_{99} downstream of stagnation ($\alpha = 0^o$) decreases from $\frac{\Lambda}{\delta_{99}} \approx 21$ at $\alpha = 10^o$ to $\frac{\Lambda}{\delta_{99}} \approx 13$ at $\alpha = 55^o$. The latter value is quite close to the ratio $\frac{\Lambda}{\delta_{99}} \approx 10$ that was found by Dullenkopf and Mayle [7] to be the most effective for increasing heat transfer.

3.2. Heat Transfer

As a dimensionless representation of the heat-flux we use the local Nusselt number Nu, which - based on D as length-scale - is defined by

$$Nu = \frac{hD}{k} = \frac{T_0}{T_\infty - T_0} \left. \frac{\partial \left(\frac{T}{T_0}\right)}{\partial \left(\frac{r}{D}\right)} \right|_{wall},$$

where k is the thermal conductivity and r is the radial coordinate with respect to the cylinder axis.

3.2.1. Time-averaged statistics

Figure 10 shows the mean local Nusselt number along the circumference at the front of the cylinder. For both the laminar 2D simulation and the 3D simulation with oncoming free-stream turbulence the maximum Nu is reached at the stagnation point, where the boundary layer is thinnest. Farther downstream, Nu gradually decreases until slightly downstream of the location where the boundary layer separates. Behind the location of separation, at the back of the cylinder, turbulent flow re-circulates (evidenced by the fine-grained instantaneous Nu-contours in Figure 13) causing a significant increase in Nu. Even though the actual turbulence level has dropped from $Tu = 30\%$ at the inflow plane to $Tu = 3.5\%$ slightly upstream of the cylinder (see Figure 6), comparing the turbulent 3D to the laminar 2D simulation, a significant increase in Nusselt number (of almost 66% at the stagnation point) can be seen in the entire front region. Also, the minimum Nu (which approximately corresponds to the location of separation) in the 3D simulation is reached approximately 10^o farther downstream as compared to the laminar simulation. This can be explained by the free-stream turbulence in the 3D simulation that energises the boundary layer and thereby delays separation.

The fluctuation-induced normal heat flux, $\overline{v'T'}$, and the total heat flux, $q_{total} = \overline{v'T'} - \frac{1}{Pr\,Re}\frac{\partial T}{\partial r}$ are shown in Figure 11 at various locations, $\alpha = 10^o, 20^o, \ldots, 50^o$, in the stagnation region of the cylinder from Simulation II. At all locations, very close to the cylinder the laminar heat flux is the sole contributor to q_{total} as the presence of the wall completely damps the wall-normal fluctuations such that $\overline{v'T'} \approx 0$. Farther away from the cylinder's surface, the fluctuation-induced normal heat flux quickly becomes the main contributor to the total heat flux. Moving downstream from the stagnation line, the viscous layer adjacent to the cylinder (identified by the lack of fluctuation-induced heat transfer) can be seen to slowly become thicker, which causes the local Nusselt number to decrease. Another remarkable result is how far heat is transported away from the cylinder by the fluctuation-induced normal heat flux: In the radial direction, $\overline{v'T'}$ only very gradually declines and heat is transported up to 0.05D away from the cylinder. From this we can draw the conclusion that turbulent diffusion of heat is a very important transport mechanism that causes to the observed increase in Nusselt number by 66% as compared to the base-line simulation.

Using data from many experiments, Dullenkopf and Mayle [9] derived a correlation,

$$Nu_a Pr^{-0.37} = 0.571 + 0.0125\,Tu_a \left\{ 1 + \frac{1.8}{[1 + (Tu_a/20)^3]} \right\}, \qquad (1)$$

between $Nu_a\,Pr^{-0.37}$ and Tu_a, where $Nu_a = \frac{Nu}{\sqrt{a_1\,Re_D}}$ is the modified Nusselt number at stagnation, a_1 is the non-dimensional strain rate that can be determined from the gradient $\frac{\partial(U/U_0)}{\partial(x/D)}$ near the stagnation point and $Tu_a = Tu\,\sqrt{Re_D/a_1}$ is the modified turbulence level - which is evaluated at $x/D = -0.8$. In Simulation II the non-dimensional strain rate and modified turbulence level are given by $a_1 \approx 3.7$ and $Tu_a \approx 0.035$, respectively. The correlation curve is shown in Figure 12, together with a number of markers representing the results obtained in Simulations I & II and in previous - lower Reynolds number - simulations by the authors of flow around and heat transfer from turbine blades and circular cylinders. Compared to the correlation curve of Dullenkopf and Mayle, all DNS results predict a slightly lower laminar heat transfer, though the rate of increase of $Nu_a\,Pr^{-0.37}$ with Tu_a is found to be in very good agreement.

To also account for the influence of the integral length-scale, Λ, on the heat transfer augmentation at stagnation, Dullenkopf and Mayle [7] replaced equation (1) by

$$Nu_a Pr^{-0.37} = 0.571 + 0.01\,Tu_\lambda, \tag{2}$$

where a dimensionless integral length scale

$$L_a = (\Lambda/D)\sqrt{a_1\,Re_D}$$

and a turbulence parameter

$$Tu_\lambda = \frac{Tu_a\,\sqrt{L_a}}{[1 + 0.004L_a^2]^{5/12}}.$$

were introduced. The integral length scale is $\Lambda \approx 0.057D$, as determined from two-point correlations of the spanwise velocity component, w, in the spanwise direction at the same location where Tu_a is evaluated. Based on this Λ, the dimensionless integral length scale becomes $L_a \approx 41.02$ so that the turbulence parameter becomes $Tu_\lambda \approx 18.6$. A direct calculation gives $Nu_a Pr^{-0.37} \approx 0.763$, while $0.571 + 0.01\,Tu_\lambda \approx 0.757$; a difference of only 1.03%.

3.2.2. Instantaneous heat transfer and temperature fields

In Figure 13, contours of the instantaneous Nusselt number, Nu along the surface of the cylinder are shown. The stagnation line is at $\alpha = 0^o$. In the stagnation region, a relatively coarse pattern consisting of streamwise elongated strips of high Nu can be seen. The strips are the footprints of impinging free-stream vortical structures that are elongated by the strongly accelerating flow around the

front of the cylinder. Downstream separation - where Nu reaches a minimum - a fine-grained pattern in the Nu-contours is obtained. This pattern reflects the presence of turbulent re-circulating flow along the entire downstream half of the cylinder.

A study of the origin of the coarse pattern in the Nu-contours that was observed along the front of the cylinder from Simulation II (see Figure 13) is presented in Figure 14. Here, a sequence of six radial cross-sections through the boundary layer at $\alpha = 0^o, 10^o, \ldots, 50^o$ - showing fluctuating velocity vectors and contours of the instantaneous temperature T - is shown. The approximate location of the edge of the boundary layer is identified by δ. The actual location of the zoomed snapshots is identified in Figure 2. As the flow moves along the surface of the cylinder, the boundary layer thickness can be seen to increase from $0.0027D$ at $\alpha = 10^o$ to $0.0045D$ at $\alpha = 20^o$. The rotating structure that is observed near $(z/D, r/D) = (0.115, 0.515)$ in the snapshots at $\alpha = 10^o, \ldots, 50^o$ corresponds to a single, slightly meandering streamwise vortical structure that is wrapped around the stagnation region of the circular cylinder by the accelerating wall-parallel streamwise flow. At the left, the counter-clockwise rotation forces cold fluid from the free-stream towards the cylinder's surface, while on the right hot fluid that originates from the cylinder's surface is swept upwards. It is this hot fluid being lifted upward that is reflected by the formation of the distinctive coarse pattern in the Nu-distribution as seen in Figure 13.

4. Conclusions

A DNS of the effects of impinging fluctuations on the heat transfer in the stagnation region of a circular cylinder has been carried out at a Reynolds number in the higher subcritical range, which is considerably higher than in other DNS. From the simulations we reach the following conclusions:

- The strongly accelerating wall-parallel flow stretches vortical structures introduced at the inflow of the 3D simulation and re-orientates them in the direction of flow as the structures approach the stagnation region of the cylinder.

- Upon impingement, the elongated vortical structures promote the transport of cold fluid from the free-stream towards the cylinder, while at the same time hot fluid is swept from the cylinder up towards the free-stream, resulting in a coarse, elongated pattern of high values of the instantaneous Nusselt number.

- Though in the viscous sublayer the thermal diffusion is found to be fully laminar, higher up in the boundary layer the fluctuation-induced wall-normal transport of heat takes over and is found to be able to transport heat well away from the surface of the cylinder (up to $0.05D$ in the radial direction), at stagnation even against the main direction of flow.

- Compared to the laminar base-line simulation, in the three-dimensional simulation with free-stream turbulence the observed fluctuation-level of $Tu = 3.5\%$ prevailing immediately upstream of the cylinder (down from $Tu = 30\%$ at the inflow plane) led to an increase in the time-averaged Nusselt number of 66% in the stagnation region.

- A very good agreement of the heat transfer results with the empirical correlations of Dullenkopf and Mayle [9, 7] was obtained.

Acknowledgements

The authors would like to thank the German Research Foundation (DFG) for funding this project and the Steering Committee for the Supercomputing Facilities in Stuttgart for granting computing time on the NEC-SX8.

References

[1] J. Kestin, P. Maeder, H. Wang, Influence of turbulence on heat transfer of heat from plates with and without pressure gradient, Int. J. Heat Mass Transfer 3 (1961) 133–154.

[2] G. Junkhan, G. Sevory, Effects of free-stream turbulence and pressure-gradient on flat plate boundary layer velocity profiles and on heat transfer, ASME J. Heat Transfer 89 (1967) 169–176.

[3] S. Wittig, A. Schulz, H. Bauer, K. Sill, Effects of wakes on heat transfer in gas turbine cascades, AGARD CP 390 (1985) 6–1–6–13.

[4] G. van Fossen, R. Simoneau, C. Ching, Influence of turbulence parameters, Reynolds number and body shape on stagnation point heat transfer, J. Heat Transfer 125 (1995) 221–231.

[5] F. Ames, C. Wang, P. Barbot, Measurements and prediction of the influence of catalytic and dry low no_x combustor turbulence on vane surface heat transfer, ASME J. Turbomachinery 125 (2003) 221–231.

[6] Z. Xiong, S. Lele, Distortion of upstream disturbances in a hiemenz boundary layer, J. Fluid Mech. 519 (2004) 201–232.

[7] K. Dullenkopf, R. Mayle, An account of free-stream-turbulence length scale on laminar heat transfer, ASME J. Turbomachinery 117 (1995) 401–406.

[8] N. Yardi, S. Sukhatme, Effect of turbulence intensity and integral length scale of a turbulent free stream on forced convection heat transfer from a circular cylinder in cross flow, in: Proceedings of 6th Int. Heat Transfer Conference, Toronto, Canada, Vol. 5, 1978, pp. 347–352.

[9] K. Dullenkopf, R. Mayle, The effects of incident turbulence and moving wakes on laminar heat transfer in gas turbines, ASME J. Turbomachinery 116 (1994) 23–28.

[10] J. Wissink, W. Rodi, Direct numerical simulation of flow and heat transfer in a turbine cascade with incoming wakes, J. Fluid Mech. 569 (2006) 209–247.

[11] Z. Xiong, S. Lele, Stagnation point flow under free-stream turbulence, J. Fluid Mech. 590 (2007) 1–33.

[12] J. Wissink, W. Rodi, Direct numerical simulation of heat transfer from the stagnation region of a heated cylinder affected by an impinging wake, J. Fluid Mech., in print.

[13] M. Breuer, W. Rodi, Large eddy simulation for complex turbulent flow of practical interest, in: E. Hirschel (Ed.), Flow simulation with high-performance computers II, Notes in Numerical Fluid Mechanics, Vol. 52, Vieweg Verlag, Braunschweig, 1996.

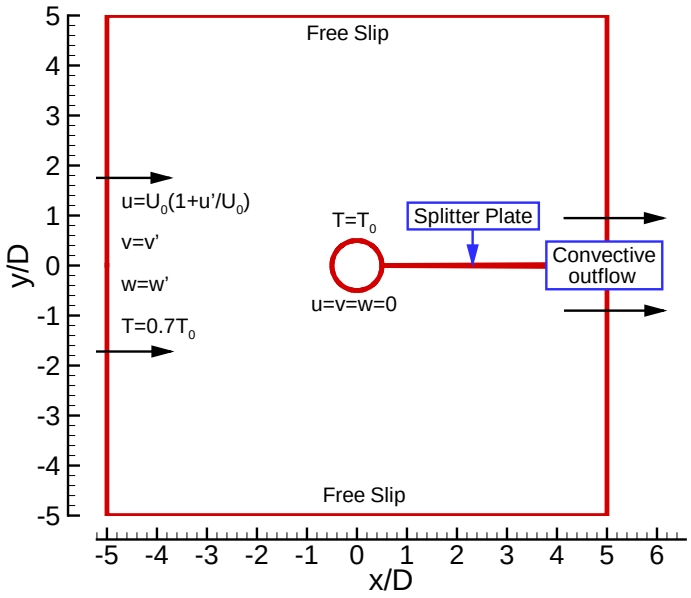
Free Slip
u=U0(1+u'/U0)
v=v'
w=w'
T=0.7T0
T=T0
Splitter Plate
Convective outflow
u=v=w=0
Free Slip
y/D
x/D
5
4
3
2
1
0
-1
-2
-3
-4
-5
-5 -4 -3 -2 -1 0 1 2 3 4 5 6

Figure 1

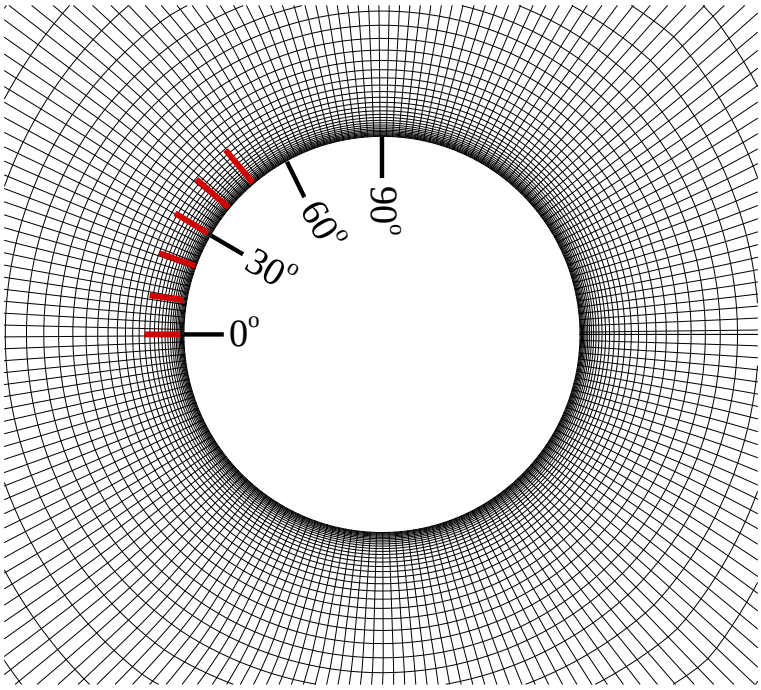

Figure 2

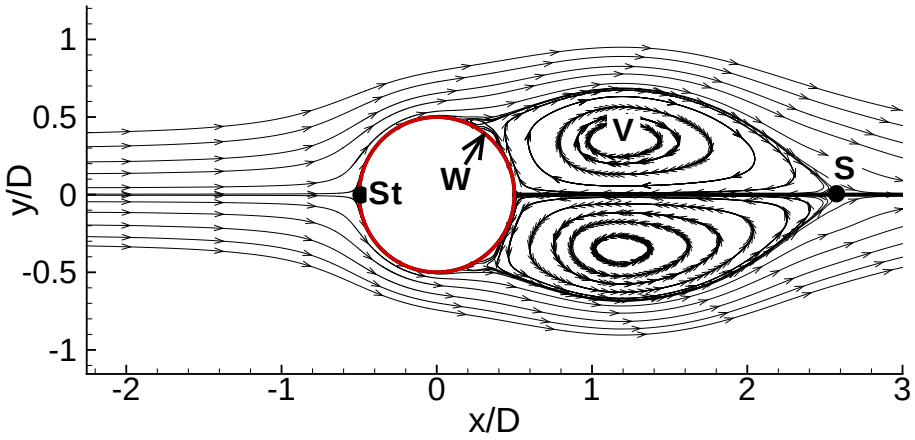

Figure 3

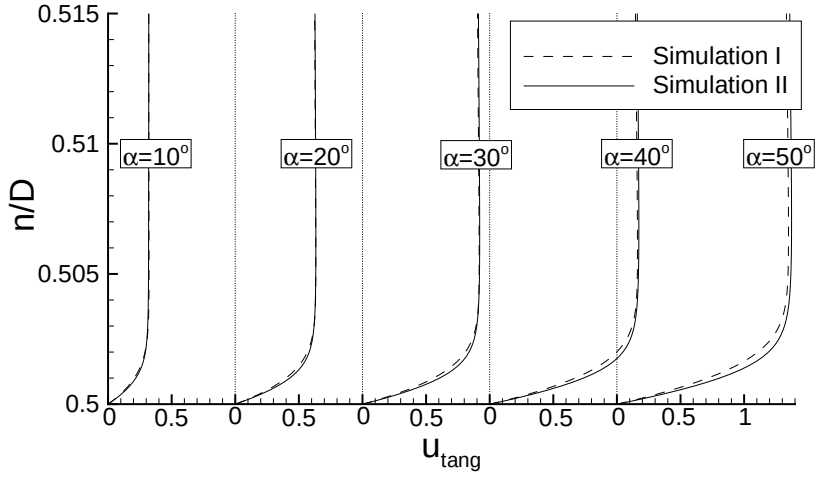
0.515
0.51
0.505
0.5
n/D
Simulation I
Simulation II
α=10°
α=20°
α=30°
α=40°
α=50°
0
0.5
0
0.5
0
0.5
0
0.5
0
0.5
1
u_tang

Figure 4

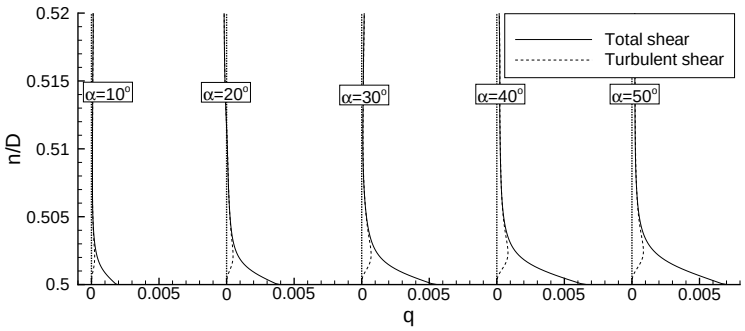
0.52
0.515
0.51
0.505
0.5
n/D
α=10°
α=20°
α=30°
α=40°
α=50°
Total shear
Turbulent shear
0
0.005
q

Figure 5

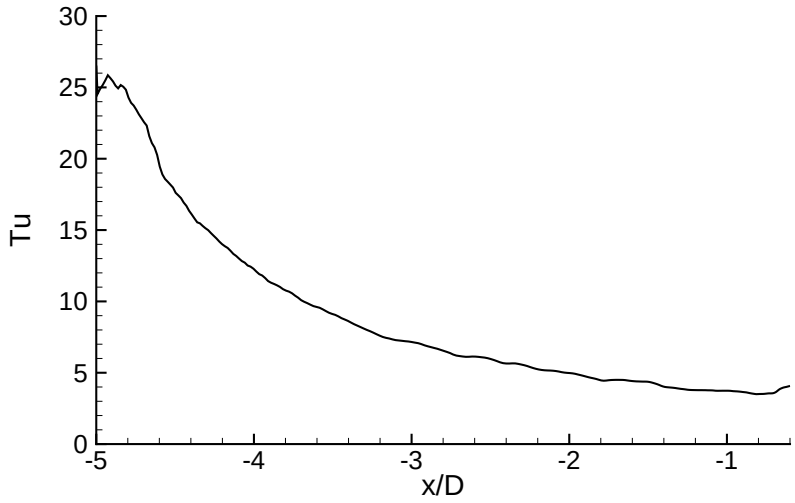

Figure 6

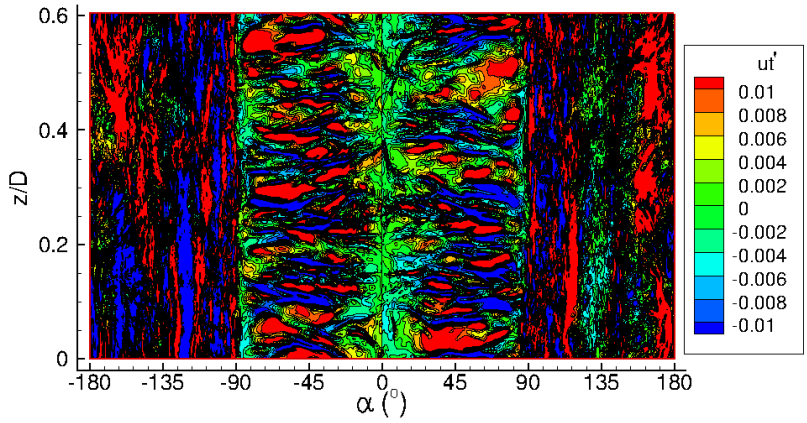
0.6
0.4
0.2
0
z/D
-180
-135
-90
-45
0
45
90
135
180
α (°)
ut'
0.01
0.008
0.006
0.004
0.002
0
-0.002
-0.004
-0.006
-0.008
-0.01

Figure 7

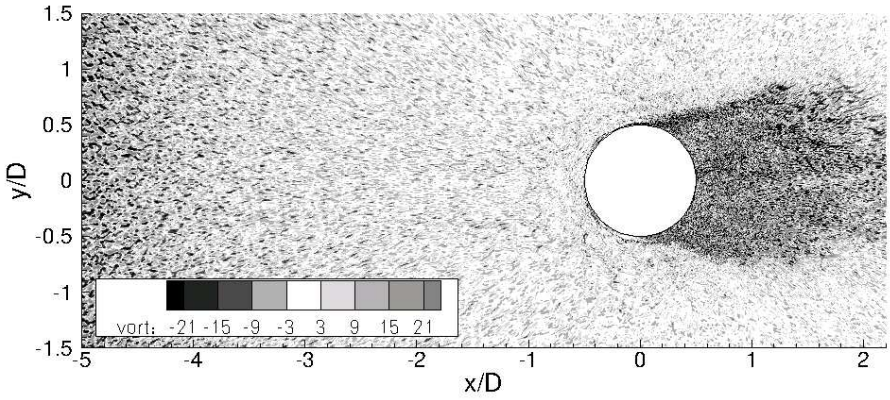

Figure 8

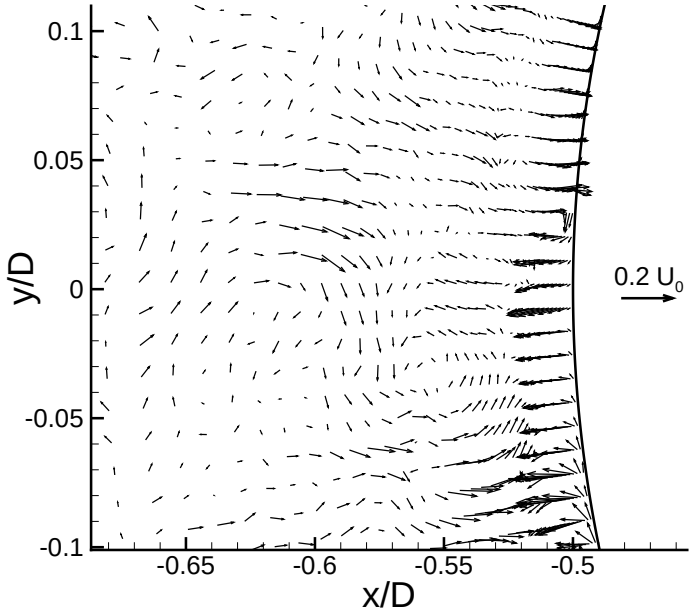

Figure 9

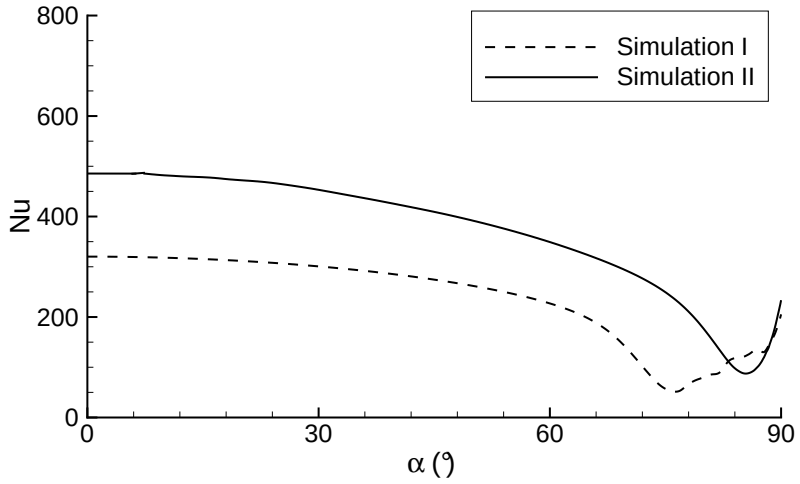

Figure 10

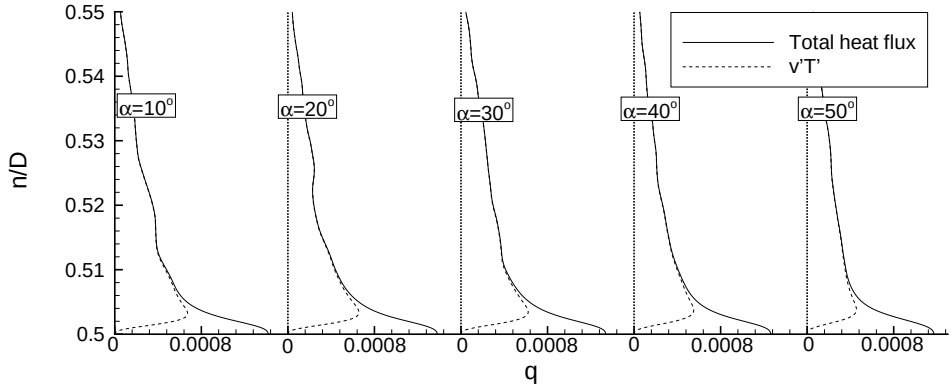
0.55
0.54
0.53
0.52
0.51
0.5
n/D
α=10°
α=20°
α=30°
α=40°
α=50°
Total heat flux
v'T'
0
0.0008
q

Figure 11

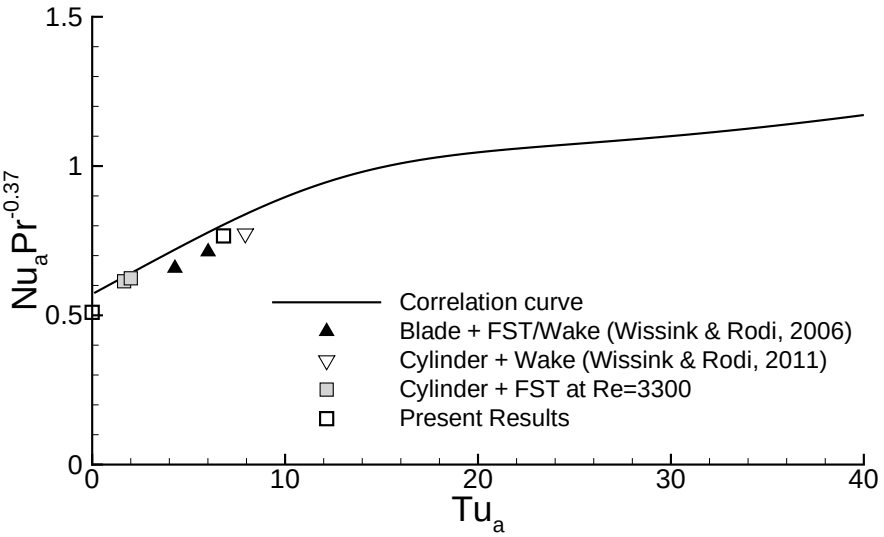
1.5
1
0.5
0
0
10
20
30
40
$Nu_a Pr^{-0.37}$
Tu_a
Correlation curve
Blade + FST/Wake (Wissink & Rodi, 2006)
Cylinder + Wake (Wissink & Rodi, 2011)
Cylinder + FST at Re=3300
Present Results

Figure 12

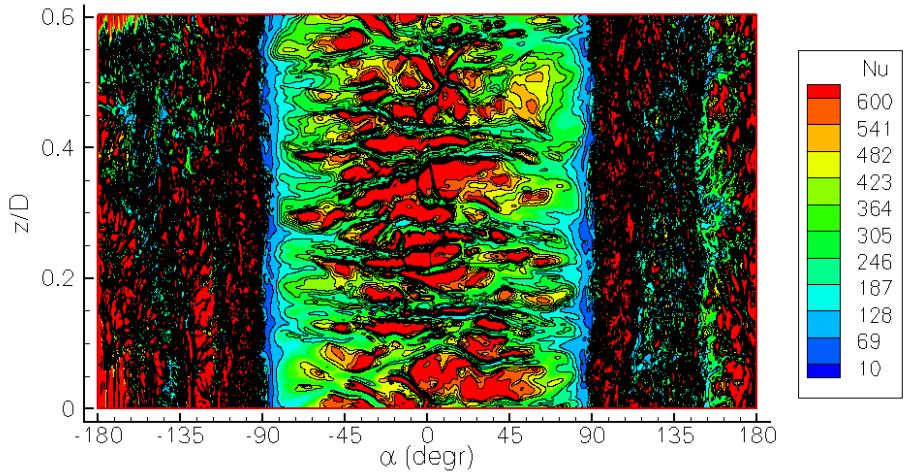
0.6
0.4
0.2
0
z/D
-180
-135
-90
-45
0
45
90
135
180
α (degr)
Nu
600
541
482
423
364
305
246
187
128
69
10

Figure 13

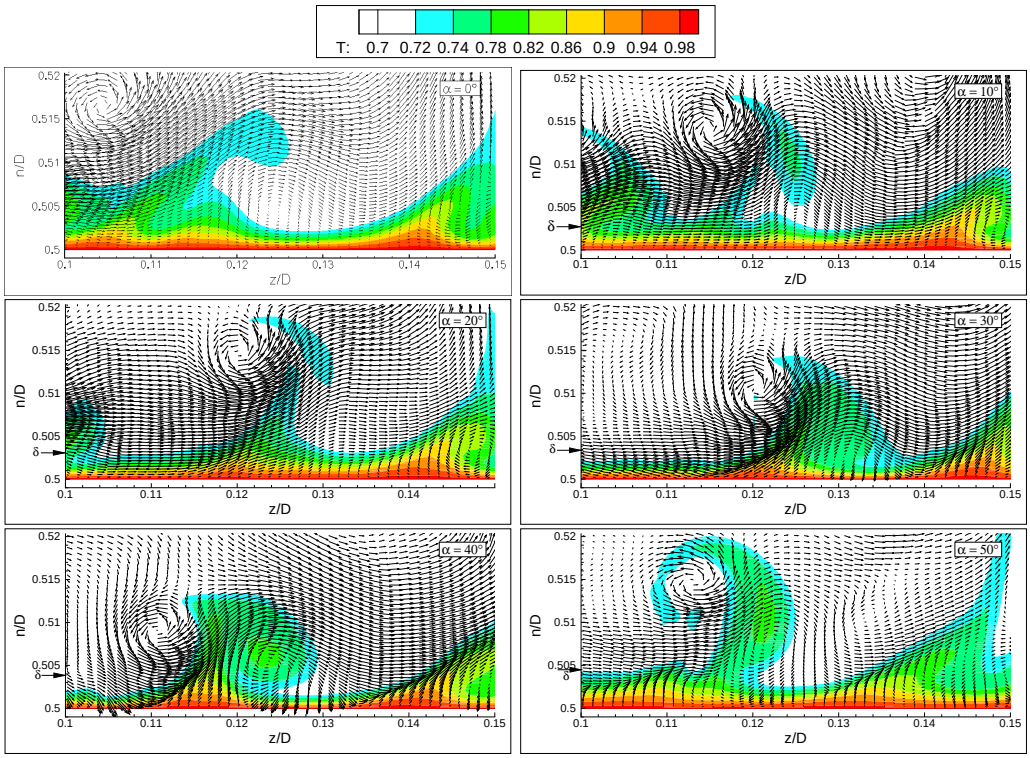

Figure 14

Figure 1: *Computational setup.*

Figure 2: *O-mesh in the vicinity of the cylinder showing every* 12^{th} *grid line.*

Figure 3: *Time-averaged streamlines at midspan from Simulation II*

Figure 4: *Profiles of the streamwise (circumferential) velocity in the boundary layer at* $\alpha = 10^o, 20^o, \ldots, 50^o$

Figure 5: *Simulation II: Total and fluctuation-induced shear stress in the stagnation region of the cylinder at* $\alpha = 10^o, 20^o, \ldots, 50^o$ *plotted against radial distance from the centre of the cylinder*

Figure 6: *Simulation II: Turbulence intensity along* $y/D = 0$ *in the inflow region*

Figure 7: *Simulation II: Contours of the circumferential velocity fluctuations in a plane at a distance of* $0.00065D$ *to the cylinder's surface*

Figure 8: *Simulation II: Instantaneous spanwise vorticity at midspan*

Figure 9: *Simulation II: Vector field of the fluctuating velocity near stagnation, showing vectors at every* 7^{th} *point in the radial and circumferential directions.*

Figure 10: *Time-averaged local Nusselt number along the circumference at the front of the cylinder*

Figure 11: *Simulation II: Total heat flux and fluctuation-induced heat flux at* $\alpha = 10^o, 20^o, \ldots, 50^o$ *in the stagnation region of the cylinder plotted against the radial distance from the centre of the cylinder*

Figure 12: *Correlation curve* Nu_a *versus* Tu_a

Figure 13: *Instantaneous Nusselt number around the cylinder from Simulation II*

Figure 14: *Simulation II: A sequence of six orthogonal cross-sections at* $\alpha = 0^o, 10^o, 20^o, 30^o, 40^o, 50^o$ *(zoomed view) originating from a single snapshot showing the fluctuating velocity vectors and contours of the instantaneous temperature.*

Sim.	$Tu\|_{in}$	Mesh	Span size
I	0.0%	$2406 \times 606 \times 4$	$0.03D$
II	30.0%	$2406 \times 606 \times 512$	$0.6D$

Table 1: Overview of the direct numerical simulations performed.